

The spectra of evolved stars at 20–25 GHz: tracing circumstellar chemistry during the asymptotic giant branch to planetary nebula transition

Yong Zhang¹, Wayne Chau², Jun-ichi Nakashima¹, Sun Kwok³

zhangyong5@mail.sysu.edu.cn

ABSTRACT

We report an unbiased radio line survey towards the circumstellar envelopes of evolved stars at the frequency range from 20 to 25 GHz, aiming to obtain a more complete unbiased picture of the chemical evolution in the final stages of stellar evolution. The observation sample includes the asymptotic giant branch (AGB) star IRC+10216, the proto-planetary nebulae (PPNs) CRL 2688 and CRL 618, and the young planetary nebula (PN) NGC 7027, representing an evolutionary sequence spanning about 10,000 years. Rotational transitions from cyanopolyynes chains and inversion lines from ammonia are detected in the AGB star and PPNs, while the PN displays several recombination lines. The different spectral behaviors of these evolved stars clearly reflect the evolution of circumstellar chemistry during the AGB-PPN-PN transitions.

Subject headings: circumstellar matter — ISM: molecules — radio lines: stars — stars: AGB and post-AGB — planetary nebulae

1. Introduction

The circumstellar envelope (CSE) of evolved stars comprises of materials that are ejected by the dying star. Observations at radio wavelengths have shown that

¹School of Physics and Astronomy, Sun Yat-Sen University, Tangjia, Zhuhai, China

²Department of Physics, University of Hong Kong, Pokfulam Road, Hong Kong, China

³Department of Earth, Ocean, and Atmospheric Sciences, University of British Columbia, Vancouver, Canada

CSEs are the synthesis site of various gas molecules which are building blocks for more complex organic compounds. Due to the evolution of the central star and variation of mass loss, the physical conditions in the CSE — such as density, temperature, and radiation field — change rapidly as an object evolves from the asymptotic giant branch (AGB) to the proto-planetary nebula (PPN) and subsequently to the planetary nebula (PN) stage. Such environmental changes facilitate the onset of different chemical reactions that spawn a plethora of molecular species. The brevity of the PPN and PN phases, $\sim 10^3$ and $\sim 10^4$ years respectively, places excellent constraints on chemical models (Kwok 2004). Understanding of the circumstellar chemistry must rely on the identification analysis of molecular features in objects at different evolutionary stages, making unbiased spectral line surveys the most ideal method to investigate conditions and composition of CSEs on a global scale (see Cernicharo et al. 2011, for a comprehensive review). However, such studies are very time-consuming, and thus have mostly focused on a few brightest objects or been performed over limited frequency ranges.

Recent technological advances in radio receivers have motivated increasing interests in performing unbiased line surveys towards CSEs, which deliver an unbiased view of the circumstellar chemistry. The observations using the same instrumental settings minimize systematic uncertainties and enable us to make a direct comparison between CSEs with different properties and at different evolutionary stages. For instance, Tenenbaum et al. (2010a,b) carried out a 1 mm spectral line survey of the O-rich CSE VY Camis Majoris and the C-rich CSE IRC+10216. These observations revealed unexpected chemical complexity in O-rich environments (Ziurys et al. 2007). More recently, Daniel et al. (2012), Gong et al. (2015) and Zhang et al. (2017) have conducted molecular line studies on IRC+10216 using the Herschel Space Observatory, the Effelsberg 100-m radio antenna and the Tian Ma Radio Telescope, respectively. In particular, the survey of Gong et al. (2015), which covered the 17.8 – 26.3 GHz frequency range, detected a total of 78 transitions from known molecular species, amongst which 23 were detected for the first time outside the solar system. Our research group has been engaged in a long-term project to perform systematic spectral line surveys in a large sample of evolved stars with comprehensive wavelength coverage (He et al. 2008; Zhang et al. 2008, 2009a,b; Chau et al. 2012; Zhang et al. 2013). In the present paper, we investigate the 20–25 GHz spectra of a sample consisting of C-rich CSEs including IRC+10216, CRL 2688, CRL 618, and NGC 7027.

Displayed in Table 1 are the physical properties of the scientific objects consolidated from a series of literature searches. Unless otherwise stipulated, all analysis in this study will be based on the parameters listed in the table.

With over 70 molecular species discovered, IRC+10216 is often considered to be an archetypal C-rich AGB (see, e.g., Cernicharo et al. 2000, 2010; He et al. 2008; Patel et al. 2011). Although its chemical uniqueness is certainly a matter for debate, the spectrum of IRC+10216 serves as a useful baseline to compare and contrast with the spectra of the other objects in studying circumstellar chemistry. CRL 2688 is a PPN that left the AGB phase approximately 200–350 years ago (Jura & Kroto 1990; Ueta et al. 2006). Its central star has an effective temperature of about 7.25×10^3 K, and is not hot enough to photoionize the CSE. Near-infrared (NIR) imaging studies show that the multipolar morphology of CRL 2688 originates from high-velocity outflows of H₂ (Latter et al. 1993; Sahai et al. 1998), and interferometric observations reveal a series of collimated CO jets that are highly correlated with the H₂ emission (Cox et al. 2000). The geometry of CRL 2688 might introduce some chemical complexity. The dust- and shock-induced chemistry probably take place in the central dusty torus and the polar direction, respectively. A wide variety of molecules — such as the silicon-bearing molecules SiO and SiS, cyanopolyynes up to HC₉N and carbon radicals up to C₆H — have been detected in CRL 2688 (Lucas et al. 1986; Truong-Bach et al. 1993; Bachiller et al. 1997a,b). Line surveys of this objects have been recently performed at 1 mm, 1.3 mm, and 3 mm windows (Park et al. 2008; Zhang et al. 2013). CRL 618 is a more evolved PPN having a central star with a higher effective temperature (3.0×10^4 K; Sánchez Contreras & Sahai 2004). It is believed to be on the verge of becoming a full-blown PN. Its morphology can be characterized by two components: a slowly expanding (19 km s^{-1}) halo component that extends to over 15–20'' with a mass of a couple of solar masses (Phillips et al. 1992; Fukasaku et al. 1994; Sánchez Contreras & Sahai 2004) and a high-velocity ($\pm 300 \text{ km s}^{-1}$) bipolar component about 3–5'' in length that is significantly less massive (Neri et al. 1992; Trammell & Goodrich 2002; Balick et al. 2013). Previous line surveys of this object cover a frequency range from 80–276 GHz (Bujarrabal et al. 1988; Pardo et al. 2004, 2005, 2007). NGC 7027 is a young PN with a hot central star ($\sim 2.19 \times 10^5$ K; Zhang et al. 2005). Surprisingly, observations show that most of the molecules can survive photodissociation by the strong UV radiation field (Edwards & Ziurys 2013). The similarity of species between diffuse clouds and PNs suggests that the “survival”

molecules are dispersed into the interstellar medium (ISM) with the expansion of the nebulae (Ziurys 2006). A comparison between the spectral properties of the four typical targets in different evolutionary stages of evolved stars can provide a more complete picture of C-rich circumstellar chemistry.

2. Observation and Data Reduction

The observations were carried out with the 45-m radio telescope at the Nobeyama Radio Observatory (NRO) during two periods: May 2010 (for IRC+10216) and February to May 2013 (for CRL 2688, CRL 618, and NGC 7027). Data were taken using the position switching mode, with on-source integration time of about 1–2 hr for each target. The receiver backend is the digital spectrometer SAM45, which provides 16-array outputs, each with 4096 spectral channels. The bandwidth and the channel spacing are 2 GHz and 448 kHz respectively. Two adjacent spectral channels were binned together, to enhance the signal-to-noise ratio, resulting in a resolution of ~ 1 MHz or 12 km s^{-1} at 25 GHz. The beam size, θ_b , and the main-beam efficiency, η_m , referenced at 23 GHz are $73''$ and 0.83, respectively. Typical system temperatures during the observations were between 90 and 180 K with instances of it increasing to over 200 K when weather conditions became less optimal. The pointing accuracy was checked every 2–3 hr by observing nearby SiO maser sources. Spectra obtained were reduced using the NewStar¹ software package. The baselines were subtracted using low-order polynomial fits to the line-free regions of the spectra. NGC 7027, a source with strong continuum emission, shows very irregular baseline curves in a few spectral regions. These ‘bad’ spectral regions were discarded for further analysis. Co-adding of the spectra resulted in a typical rms level of ~ 5 mK with a velocity resolution 12 km s^{-1} for IRC+10216 and CRL 2688. The rms noises are somewhat higher for CRL 618 and NGC 7027 due to the shorter cumulative integration time.

¹<http://www.nro.nao.ac.jp/nro45mrt/obs/newstar>

3. Observational Results

Figure 1 displays the reduced spectra of IRC+10216, CRL 618, CRL 2688, and NGC 7027, while the zoomed-in spectra of the four objects are presented in Figure 2. These spectra are arranged in an evolutionary sequence from AGB to PPN to PN phases so that one can directly compare and contrast between spectra of objects at different dynamical ages. A total of 37 spectral features, including molecular emission and absorption as well as recombination lines, are positively detected in the four objects. Line identification relied on cross-referencing the spectra with various catalogues of transition data. Catalogues referenced by the present study include the National Institute of Standards and Technology (NIST) Recommended Rest Frequencies for Observed Interstellar Molecular Microwave Transitions² (Lovas 2004), the JPL Catalogue of Molecular Spectroscopy³ (Pickett et al. 1998) and the CDMS catalogue⁴ (Müller et al. 2001, 2005). As a general rule of thumb, positive detection refers to features that have a peak intensity that is at least three times the rms level of its immediate spectral vicinity. Features having the signal-to-noise of 1–2 are regarded as marginal detections. The presence of these marginal detections can be argued based on other merits such as the positive detection of other transitions from the same molecular carrier within the CSE as well as detection by previous studies.

The NRO observation of IRC+10216 resulted in the detection of rotational lines from cyanopolyne and ammonia spectral features, including the $J = 8 - 7$ and $9 - 8$ lines from HC_5N , the $J = 18 - 17$, $19 - 18$, $20 - 19$, $21 - 20$ and $J = 22 - 21$ lines from HC_7N , as well as the $J - K = 1 - 1$ from NH_3 . The recent work can be regarded as an extension to Kawaguchi et al. (1995) who performed a NRO observation of IRC+10216 in the frequency range from 28–50 GHz. Measurements including peak and integrated intensities, line widths measured in full width at zero intensity (FWZI), and characteristic rms level are presented in Table 2. The FWZI was measured from the distance in velocity space between the zero points of a given feature. Because of its sensitivity to line blending, fine-structure lines as well as the

²<https://physics.nist.gov/cgi-bin/micro/table5/start.pl>

³<https://spec.jpl.nasa.gov/ftp/pub/catalog/catform.html>

⁴<http://www.astro.uni-koeln.de/cgi-bin/cdmssearch>

selection of zero points, the FWZI is not necessary equal to two times of the terminal velocity. From the table and the zoomed-in profiles in Figure 3, it is apparent that the strength of the NH_3 $J - K = 1 - 1$ feature is weak relative to those of the cyanopolyynes. We did not detect higher order ammonia transitions in IRC+10216. Generally, HC_5N lines are stronger than HC_7N lines, and show less symmetric profiles. As noted in Chau et al. (2012), a similar trend, namely that the profile asymmetry is less for the larger molecule, is observed when comparing the HC_3N and HC_5N transitions at a higher frequency regime.

In previous studies, the longer cyanopolyne chain HC_9N has been observed (see, e.g., Bell et al. 1992; Truong-Bach et al. 1993), four of which lie within our frequency range. However, HC_9N in IRC+10216 is less abundant than HC_7N by one order of magnitude (Truong-Bach et al. 1993), and thus is not expected to be detected at our sensitivity level. Based on the observations performed with the 100-m radio telescope at Effelsberg, which has a HPBW of $36''.5$ at 15 GHz, Truong-Bach et al. (1993) obtained that the HC_9N lines have a brightness temperature of 11–16 mK. Considering the beam-dilution effect, these lines in our spectra should have antenna temperatures of $T_A < 9$ mK, well below the 3σ detection limits.

The 20-25 GHz spectrum of CRL 2688 is quite similar with that of IRC+10216. Emission lines from HC_5N , HC_7N , and NH_3 are clearly detected. However, their intensities are different from those in IRC+10216 (see Table 2 for a comparison). Comparing to IRC+10216, CRL 2688 exhibits stronger NH_3 lines, weaker cyanopolyne lines, and larger $\text{HC}_7\text{N}/\text{HC}_5\text{N}$ intensity ratios. Profiles of the most prominent lines in CRL 2688 are presented in Figure 3 with their counterparts in the spectrum of IRC+10216 superimposed. The profiles associated with IRC+10216 have been scaled by a factor of 0.5. It is apparent that the HC_5N lines in CRL 2688 show a double-peak structure on which the red-ward peak is stronger, suggesting that these low-frequency HC_5N transitions are optically thin and primarily originate from the outer region of a detached envelope. Such a behaviour is typical for expanding circumstellare envelopes (e.g. Chau et al. 2012). The central dip is not seen in the HC_5N line profiles of IRC+10216 in that this object has a smaller angular extent. The detected NH_3 features are groups of unresolved hyperfine structure of the $J - K = 1 - 1$, $2 - 2$, $3 - 3$ and $4 - 4$ transitions. The detections of the $J - K = 1 - 1$ and $2 - 2$ transitions in CRL 2688 have reported by Nguyen-Q-Rieu (1984). In IRC+10216, though several NH_3 lines have been discovered previously (Gong et al. 2015; Schmidt et al. 2016), we

only detect the strongest $J-K = 1-1$ transition. As shown in Figure 3, the intensity of the NH_3 $J-K = 1-1$ line is $\sim 63\%$ less than that of the HC_7N $J = 21-20$ HC_7N line in IRC+10216, while its intensity is $\sim 72\%$ more than that of the same HC_7N line in CRL 2688. Together with the absence of other NH_3 transitions in IRC+10216, this ostensibly indicates that NH_3 is enhanced as an object evolves from the AGB to the PPN phase.

The 20–25 GHz spectrum of CRL 618 reveals NH_3 absorption features of transitions from $J-K = 1-1$ to $6-6$. No cyanopolyynes are detected with our sensitivity. The profiles of these features are presented in Figure 4. All of these lines are centered at negative velocities with respect to the local standard of rest, and are composed of two components, wide and narrow ones. The observations of NH_3 features in CRL 2688 and CRL 618 have been reported by Truong-Bach et al. (1988) and Martin-Pintado & Bachiller (1992). Our measurements are consistent with these prior observations.

The 20–25 GHz spectrum of NGC 7027 does not reveal any molecular species. However, we detected strong recombination lines from hydrogen and much weaker recombination lines from helium. Their rest frequencies, brightness temperatures, integrated intensities and line widths are listed in Table 3. The line profiles are displayed in Figure 5. The absence of molecular lines and the presence of recombination lines are presumably brought forth by the stronger radiation field resulting from the higher temperature of the central star.

4. Analysis and Discussions

4.1. Cyanopolyynes

Cyanopolyynes is a family of linear chain molecules with a CN radical end. The large dipole moment of the CN radical leads to intense rotation emission of cyanopolyynes molecules, and thus the search for the cyanopolyynes species in interstellar and circumstellar environments has attracted great interests. The longest cyanopolyynes molecule in space is HC_9N that was detected in IRC+10216. The relative abundances of cyanopolyynes compounds can provide important insights on circumstellar chemistry (Pardo et al. 2005). Cyanopolyynes molecules in the PPN

CRL 2688 are examined via rotational analysis. Under the assumption of optically thin and local thermal equilibrium (LTE), the population of the energy states are related to the integrated intensity through the Maxwell-Boltzmann distribution as follows:

$$\ln \frac{N_u}{g_u} = \ln \frac{3k \int T_S dv}{8\pi^3 \nu \mu^2 S} = \ln \frac{N}{Q} - \frac{E_u}{kT_{\text{ex}}}, \quad (1)$$

where $\mu^2 S$ is the square of the dipole moment multiplied by the line strength, N_u , g_u , and E_u are the population, degeneracy, and excitation energy of the upper level, ν is the line frequency, and Q is the rotational partition function, which is in general a function of the excitation temperature, T_{ex} . Here, the integrated intensity $\int T_S dv$ refers to that of the source brightness temperature, T_S , which is computed from the antenna temperature by accounting for the main beam efficiency, η , and beam dilution using the following equation:

$$T_S = \frac{1}{\eta} \frac{\theta_b^2 + \theta_S^2}{\theta_S^2} T_A^*, \quad (2)$$

where θ_b and θ_S are the half power beam width (HPBW) and angular size of the source, respectively. The η value is taken to be 0.87 while θ_b is found to be 61''3–66''8 for the frequency range surveyed by linearly extrapolating values in Kawaguchi et al. (1995). With the integrated intensities obtained from the observational data, the left-hand-side of Equation (1) can be plotted against E_u/k to create rotational diagrams. Taking the inverse of the slope of the linear regression of such plot yields the excitation temperature. Presented in Figure 6 are the rotational diagrams of the cyanopolyne molecules detected in CRL 2688. Since the present survey only covers the low energy range and the thermal structure within the CSE is often stratified, data points from previous high-frequency surveys (Zhang et al. 2013; Chau et al. 2012) have been concatenated with those from the present study for a more reliable estimate of the excitation temperatures and column densities. Results from rotational analysis of cyanopolyne emission from CRL 2688 and IRC+10216 are presented in Table 4. Also listed in the table are the fractional abundances with respect to H_2 , which are computed using the formula given by Olofsson (1996),

$$f_X = 1.7 \times 10^{-28} \frac{v_e \theta_b D}{\dot{M}_{\text{H}_2}} \frac{Q(T_{\text{ex}}) \nu_{ul}^2}{g_u A_{ul}} \frac{e^{E_l/kT_{\text{ex}}} \int T_R dv}{\int_{x_i}^{x_e} e^{-4 \ln 2x^2} dx}, \quad (3)$$

where the expansion velocity v_e is in km s^{-1} , the distance D in pc and the mass loss rate \dot{M}_{H_2} in $M_\odot \text{ yr}^{-1}$ can be obtained from Table 1, $\int T_R dv$ is in K km s^{-1} , the

expansion velocity v_e is in km s^{-1} , ν_{ul} is the line frequency in GHz, g_u is the statistical weight of the upper level, A_{ul} is the Einstein coefficient for the transition, E_l is the energy of the lower level, and $x_{i,e} = R_{i,e}/(\theta_b D)$ with R_i and R_e the inner radius and outer radius of the shell taken from Woods et al. (2003).

In Figure 7, we compare the 22–25 GHz spectrum of CRL 2688 with that of IRC+10216. Figure 7 plots the integrated intensity ratios between the two objects after adjusting for difference in the effects of beam dilution by a factor of $(1 + \theta_b^2/\theta_{\text{CRL2688}}^2) / (1 + \theta_b^2/\theta_{\text{IRC+10216}}^2)$ on a logarithmic scale. The angular size of the objects are taken to be $\theta_{\text{CRL2688}} = 20''$ and $\theta_{\text{IRC+10216}} = 30''$ (Fukasaku et al. 1994). As displayed in the figure, the integrated intensity ratios of the different transitions lie within the region from 0.27 to 0.63 and have a mean value of about 0.41, in approximate agreement with the mean ratio of high-frequency lines derived in Zhang et al. (2013). There is evidence showing that the $\text{HC}_7\text{N}/\text{HC}_5\text{N}$ ratio is enhanced in CRL 2688 compared to IRC+10216, suggesting that the linear cyanopolyne molecules have been quickly reprocessed to longer cyanopolyne chains during the AGB-PPN transition.

4.2. Ammonia

The detection of ammonia in circumstellar environments is intriguing as ammonia chemistry is possibly related to the formation of amino acids, the basic building blocks of life. Recent observations show that circumstellar ammonia is much richer than theoretical predictions (i.e. Wong et al. 2018). In the present surveys, ammonia is observed in IRC+10216 and CRL 2688 in emission, as well as in CRL 618 in absorption. As shown Figure 3, the CRL 2688 exhibits an enhancement of the $\text{NH}_3/\text{HC}_7\text{N}$ ratio compared to IRC+10216. Our observations are consistent with previous works (Kwok et al. 1981; Nguyen-Q-Rieu 1984; Truong-Bach et al. 1988; Martin-Pintado & Bachiller 1992). Although the existence of NH_3 in CSEs has been well established, its origin is not yet completely understood (Hasegawa et al. 2006). Interferometric observations of CRL 2688 show that NH_3 emission is mostly confined in a central disk-like structure, while HC_7N emission arises in an extended halo, suggesting that the chemistry processes of the two molecules are different (Nguyen-Q-Rieu et al. 1986). In cold low-density environments, there is no efficient gas-phase

reaction to initiate the chemistry of N-bearing species. In current models of CSE chemistry Li et al. (2016), NH_3 is qualitatively assumed to have been formed in stellar atmospheres, and would be processed into other N-bearing species in extended CSE. The enhancement of NH_3 in CRL 2688 suggests that other mechanisms, such as shock-induced endothermic reactions and solid surface reactions, might be responsible for the formation of NH_3 during the AGB-PPN evolution. It is indeed found that NH_3 emission is associated with shocked gas (Dinh-V-Trung et al. 2009). The initialization of nitrogen species chemistry in post-AGB stage can also be inferred by the high abundance of N_2H^+ in NGC 7027 (Zhang et al. 2008). Through a non-LTE modeling for NH_3 in IRC+10216, Gong et al. (2015) derived a kinetic temperature of 70 K. The $\text{NH}_3(2,2)/(1,1)$ integrated ratio in CRL 2688 is 0.68, a value very close to that in IRC+10216 obtained by Gong et al. (2015) (0.73). This suggests that the NH_3 emitting regions in the two objects have a similar kinetic temperature.

The NH_3 feature in CRL 618 appears in absorption because there is a compact ionized region in its center providing strong continuum emission by free-free transitions. Following Martin-Pintado & Bachiller (1992), we examined the ammonia absorption features by assuming that they originate from two distinct components of the CSE. While the broad absorption features at approximately -55 km s^{-1} are associated with a high-velocity wind, the much narrower components at around -27 km s^{-1} are associated with a hot clump that is slower-moving. The narrow component is detectable in all NH_3 features except the one associated with the $J - K = 1 - 1$ transition, and becomes more prominent for higher order transitions. By contrast, the broad component becomes less perceptible for increasing $J - K$ values to the point where it is barely visible in the $J - K = 5 - 5$ and $6 - 6$ transitions as shown in Figure 4. From such observations, it is ostensible that the narrow component is from a much more energetic region that is capable of populating higher energy states that are left unpopulated in the region associated with the broad absorption component. The broad and narrow NH_3 features in CRL 618 are measured by fitting a Gaussian profile to each of the components, and the results are presented in Table 5. Since the absorption features are yet to be saturated, the lines remain in the optically thin regime — implying that the column density of each state is linearly proportional to the equivalent width. The column density of each $J - K$ level, $N_{J,K}$, can then be approximated from the equivalent width, W_ν , using

the equation (Draine 2011)

$$W_\nu \approx \left(\frac{1}{4\pi\epsilon_0} \frac{e^2}{m_e c} \right) f_{lu} \times N_{J,K}, \quad (4)$$

where e is the electronic charge, m_e is the mass of the electron, and f_{ul} is the oscillator strength. The resulting column densities presented in Table 6 are in good agreement with results of Martin-Pintado & Bachiller (1992).

We also employed rotational diagram analysis to estimate the excitation temperature and the total column density of the NH_3 molecule in CRL 618. Figure 8 presents the rotation diagram. It is evident from the figure that the broad absorption component cannot be characterized with a single rotation temperature. This suggests a stratification of the absorption region where the higher energy states are only populated in the warmer areas within the region. The narrow absorption feature is, on the other hand, well described by a single rotational temperature. Such characteristic supports the notion that the absorption region associated with the narrow features is compact in nature and can be well approximated by the LTE assumption.

Ammonia has been detected in diffuse clouds in absorption against bright background sources (Liszt et al. 2006). Our sample observations suggest that ammonia can be rapidly synthesized during the AGB-PPN transition. The produced ammonia molecules then are gradually mixed with the diffuse ISM, and can probably provide the starting materials for life, as suggested by Ziurys et al. (2009).

4.3. Recombination Lines

As presented in Figure 5, a total of 12 hydrogen and helium recombination features are detected or are marginally detected in the 20–25 GHz spectrum of NGC 7027. The peak and integrated intensities as well as the line width are listed in Table 3 along with the characteristic rms level in the region where the line resides. The mean widths of the $\text{Hn}\alpha$, $\text{Hn}\beta$ and $\text{Hen}\alpha$ lines, namely 34 ± 5 , 40 ± 10 and 43 : km s^{-1} respectively, are found to be in reasonable agreement with those associated with lower- n transitions reported in Zhang et al. (2008). The $\text{Hen}\alpha/\text{Hn}\alpha$ intensity ratio is about 0.18 ± 0.07 , roughly consistent with the He/H abundance ratio of this PN obtained by Zhang et al. (2008).

Recombination lines are not detected in CRL 618 although this PPN has a central ionized region. The spectral energy distributions constructed by Arnaud et al. (2014) show that the 20–25 GHz continuum emission of CRL 618 is about 100 times fainter than that of NGC 7027. The flux ratio between free-free and bound-bound emission is only weakly dependent on the electron temperature and density. Accordingly, if CRL 618 and NGC 7027 have the same line-to-continuum ratio, the peak intensities of radio recombination lines in CRL 618 should be lower than 2 mK, which is well below the rms level achieved in the present observations. Moreover, the central ionized region of CRL 618 is much more compact than that of NGC 7027, and thus its observations suffer from more severe effect from the beam dilution. Therefore, it is extremely difficult to detect radio recombination lines in CRL 618.

5. Summary

In this paper, we present an unbiased survey for IRC+10216, CRL 2688, CRL 618 and NGC 7027 in the 20–25 GHz frequency region, aiming to obtain an unbiased view of circumstellar chemistry during the AGB-PPN-PN evolution. Under our detection sensitivity, we do not detect new species and unexpected lines in the surveyed frequency range. Emission lines from cyanopolyynes and ammonia are detected in IRC+10216 and CRL 2688. The spectra of CRL 618 and NGC 7027 are dominated by ammonia absorption features and bright radio recombination lines, respectively. From our observations, we can draw the following picture for circumstellar chemistry. During the AGB-PPN transition, the cyanopolyne chains are continuously generated, while ammonia is abruptly enhanced through a trigger that might be related to the fast stellar winds of PPNs. At the onset of PPN-PN stage, a considerable number of molecules carried by fast stellar winds rapidly escape from the destruction of the increasingly harder UV radiation from the central stars. These molecules gradually cool down, become invisible, and are dispersed into the ISM.

We are grateful to the anonymous referee for her/his constructive comments that contributed to improve the manuscript. We thank Shuji Deguchi, Bosco H. K. Yung, and the staff at NRO for their assistance during the observations. The 45-m radio telescope is operated by Nobeyama Radio Observatory, a branch of National As-

tronomical Observatory of Japan. This work was supported by National Science Foundation of China (NSFC, Grant No. 11973099), and a grant to SK from the Natural and Engineering Research Council of Canada.

REFERENCES

- Arnaud, M., Atrio-Barandela, F, Aumont, J., et al. 2014, *A&A*,
- Bachiller, R., Forveille, T., Huggins, P. J., & Cox, P. 1997a, *A&A*, 324, 1123
- Bachiller, R., Fuente, A., Bujarrabal, V., Colomer, F., Loup, C., Omont, A., & de Jong, T. 1997b, *A&A*, 319, 235
- Balick, B., Huarte-Espinosa, M., Frank, A., Gomez, T., Alcolea, J., Corradi, R. L. M., & Vinković, D. 2013, *ApJ*, 772, 20
- Bell, M. B., Avery, L. W., MacLeod, J. M., & Matthews, H. E. 1992, *ApJ*, 400, 551
- Beiging, J. H., Wilner, D., & Thronson, Jr., H. A. 1991, *ApJ*, 379, 271
- Bujarrabal, V., Gomez-Gonzalez, J., Bachiller, R., & Martin-Pintado, J. 1988, *A&A*, 204, 242
- Cernicharo, J., Guélin, M. & Kahane, C. 2000, *A&AS*, 142, 181
- Cernicharo, J., Waters, L. B. F. M., Decin, L., et al. 2010, *A&A*, 521, L8
- Cernicharo, J., Agúndez, M. & Guélin, M. 2011, in *IAU Symp. 280 The Molecular Universe*, J. Cernicharo, & R. Bachiller (eds), ASP, p. 237
- Chau, W., Zhang, Y., Nakashima, J., Deguchi, S., & Kwok, S. 2012, *ApJ*, 760, 66
- Daniel, F., et al. 2012, *A&A*, 542, A37
- Dinh-V-Trung, Chiu, P. J., & Lim, J. 2009, *ApJ*, 700, 86
- Draine, B. T. 2011, *Physics of the Interstellar and Intergalactic Medium* (Princeton, NJ: Princeton Univ. Press)

- Cox, P., Lucas, R., Huggins, P. J., Forveille, T., Bachiller, R., Guilloteau, S., Mail-
lard, J. P., & Omont, A. 2000, *A&A*, 353, L25
- Edwards, J. L., & Ziurys, L. M. 2013, *ApJ*, 770, L5
- Fukasaku, S., Hirahara, Y., Masuda, A., et al. 1994, *ApJ*, 437, 410
- Gong, Y., Henkel, C., Spezzano, S., Thorwirth, S., Menten, K. M., Wyrowski, F.,
Mao, R. Q., & Klein, B. 2015, *A&A*, 574, A56
- Hasegawa, T. I., & Kwok, S. 2001, *ApJ*, 562, 824
- Hasegawa, T. I., Kwok, S., Koning, N., et al. 2006, *ApJ*, 637, 791
- He, J. H., Dinh, V. T., Kwok, S., et al. 2008, *ApJS*, 177, 275
- Huang, Z.-Y., et al. 2010, *ApJ*, 722, 273
- Ishigaki, M. N., Parthasarathy, M., Reddy, B. E., et al. 2012, *MNRAS*, 425, 997
- Jura, M., & Kroto, H. 1990, *ApJ*, 351, 222
- Kawaguchi, K., Kasai, Y., Ishikawa, S.-i., & Kaifu, N. 1995, *PASJ*, 47, 853
- Kwok, S., Bell, M. B., & Feldman, P. A. 1981, *ApJ*, 247, 125
- Kwok, S. 2004, *Nature*, 430, 26
- Latter, W. B., Hora, J. L., Kelly, D. M., Deutsch, L. K., & Maloney, P. R. 1993, *AJ*,
106, 260
- Lovas, F. J. 2004, *Journal of Physical and Chemical Reference Data*, 33, 177
- Li, X., Millar, T. J., Heays, A. N., et al. 2016, *A&A*, 588, A4
- Liszt, H. S., Lucas, R., & Pety, J. 2006, *A&A*, 448, 253
- Lucas, R., Omont, A., Guilloteau, S., & Nguyen-Q-Rieu. 1986, *A&A*, 154, L12
- Martin-Pintado, J., & Bachiller, R. 1992, *ApJ*, 391, L93
- Masson, C. R. 1989, *ApJ*, 336, 294

- Müller, H. S. P., et al. 2001, *A&A*, 370, L49
- Müller, H. S. P., et al. 2005, *Journal of Molecular Structure*, 742, 215
- Neri, R., Garcia-Burillo, S., Guélin, M., Cernicharo, J., Guilloteau, S., & Lucas, R. 1992, *A&A*, 262, 544
- Nguyen-Q-Rieu, Graham, D., & Bujarrabal, V. 1984, *A&A*, 138, L5
- Nguyen-Q-Rieu, Winnberg, A., & Bujarrabal, V. 1986, *A&A*, 165, 204
- Olofsson, H. 1996, in *IAU Symp. 178, Molecules in Astrophysics: Probes & Processes*, ed. E. van Dishoeck (Dordrecht: Kluwer), 457
- Pardo, J. R., Cernicharo, J., & Goicoechea, J. R. 2005, *ApJ*, 628, 275
- Pardo, J. R., Cernicharo, J., Goicoechea, J. R., Guélin, M., & Asensio Ramos, A. 2007, *ApJ*, 661, 250
- Pardo, J. R., Cernicharo, J., Goicoechea, J. R., & Phillips, T. G. 2004, *ApJ*, 615, 495
- Park, J. A., Cho, S.-H., Lee, C. W., & Yang, J. 2008, *AJ*, 136, 2350
- Patel, N. A., Young, K. H., Gottlieb, C. A., et al. 2011, *ApJS*, 193, 17
- Phillips, J. P., Williams, P. G., Mampaso, A., & Ukita, N. 1992, *A&A*, 260, 283
- Pickett, H. M., Poynter, R. L., Cohen, E. A., Delitsky, M. L., Pearson, J. C., & Müller, H. S. P. 1998, *J. Quant. Spectrosc. Radiat. Transfer*, 60, 883
- Sahai, R., et al. 1998, *ApJ*, 493, 301
- Sánchez Contreras, C., & Sahai, R. 2004, *ApJ*, 602, 960
- Schmidt, M. R., He, J. H., Szczerba, R., et al. 2016, *A&A*, 592, A131
- Storey, P. J., & Hummer, D. G. 1995, *MNRAS*, 272, 41
- Tenenbaum, E. D., Dodd, J. L., Milam, S. N., Woolf, N. J., & Ziurys, L. M. 2010a, *ApJ*, 720, L102

- Tenenbaum, E. D., Dodd, J. L., Milam, S. N., Woolf, N. J., & Ziurys, L. M. 2010b, *ApJS*, 190, 348
- Trammell, S. R., & Goodrich, R. W. 2002, *ApJ*, 579, 688
- Truong-Bach, Graham, D., & Nguyen-Q-Rieu. 1988, *A&A*, 199, 291
- Truong-Bach, Graham, D., & Nguyen-Q-Rieu. 1993, *A&A*, 277, 133
- Ueta, T., Murakawa, K., & Meixner, M. 2006, *ApJ*, 641, 1113
- Wong, K. T., Menten, K. M., Kamiński, T., et al. 2018, *A&A*, 612, A48
- Woods, P. M., Schöier, F. L., Nyman, L.-A., & Olofsson, H. 2003, *A&A*, 402, 617
- Zhang, X. Y., Zhu, Q. F., Li, J., Chen, X., Wang, J. Z., & Zhang, J. S. 2017, *VizieR Online Data Catalog*, 360
- Zhang, Y., Kwok, S., & Dinh, V. T. 2008, *ApJ*, 678, 328
- Zhang, Y., Kwok, S., & Dinh, V. T. 2009a, *ApJ*, 691, 1660
- Zhang, Y., Kwok, S., & Nakashima, J. 2009b, *ApJ*, 700, 1262
- Zhang, Y., Kwok, S., Nakashima, J., Chau, W., & Dinh, V. T. 2013, *ApJ*, 773, 71
- Zhang, Y., Liu, X.-W., Luo, S.-G., Pequignot, D., & Barlow, M. J. 2005, *A&A*, 442, 249
- Ziurys, L. M. 2006, *Proceedings of the National Academy of Science*, 103, 12274
- Ziurys, L. M., Halfen, D. T., & Woolf, N. J. 2009, *Bioastronomy 2007: Molecules, Microbes and Extraterrestrial Life*, 420, 59
- Ziurys, L. M., Milam, S. N., Apponi, A. J., & Woolf, N. J. 2007, *Nature*, 447, 1094

Table 1. Properties of the sources.

	IRC+10216	CRL 2688	CRL 618	NGC 7027
Object type	AGB	PPN	PPN	PN
R.A. ^a	09:47:57.406	21:02:18.27	04:42:53.64	21:07:01.593
Dec. ^a	+13:16:43.56	+36:41:37.0	+36:06:53.4	+42:14:10.18
P (days) ^{b,f}	630	91
L (L_{\odot}) ^{b,g,k,l}	9600	3300	10000	8100
D (pc) ^{b,h,k,l}	120	420	900	880
T_* (K) ^{b,e,g,l,o}	2.5×10^3	7.25×10^3	3.0×10^4	2.19×10^5
V_{LSR} (km s^{-1}) ^{c,e,j}	-26.4	-32	-24	25
v_e (km s^{-1}) ^{c,d,i}	14.5	19	19	30
\dot{M} ($M_{\odot} \text{ yr}^{-1}$) ^{c,d,i}	1.2×10^{-5}	1.4×10^{-4}	6.7×10^{-5}	1.1×10^{-4}
θ_s (") ^{c,m,n}	30	20	20	70

^a FK5 coordinate obtained from the SIMBAD Astronomical Database.

^b Pulsation period, stellar luminosity, distance, and stellar temperature of IRC+10216 obtained from Woods et al. (2003).

^c LSR velocity, expansion velocity, mass-loss rate, and angular size of CRL 2688, and CRL 618 obtained from Fukasaku et al. (1994).

^d Expansion velocity and mass-loss rate of IRC+10216 obtained from Woods et al. (2003).

^e Stellar temperature and LSR velocity of IRC+10216 obtained from He et al. (2008).

^f Pulsation period of CRL 2688 obtained from The International Variable Star Index.

^g Stellar luminosity and stellar temperature of NGC 7027 obtained from Zhang et al. (2005).

^h Distance of NGC 7027 adopted from Masson (1989).

ⁱ Mass-loss rate, and expansion velocity of NGC 7027 obtained from Zhang et al. (2008).

^j LSR velocity of NGC 7027 adopted from Huang et al. (2010).

^k Luminosity and distance of CRL 2688 obtained from Ueta et al. (2006).

^l Luminosity, distance and temperature of CRL 618 adopted from Sánchez Contreras & Sahai (2004).

^m Angular size of IRC+10216 and CRL 618 adopted from Fukasaku et al. (1994) and Sánchez Contreras & Sahai (2004), respectively.

ⁿ Angular size of the molecular emission region of NGC 7027 obtained from Bieging et al. (1991). The ionized region of the PN is closer to $10''$ (Hasegawa & Kwok 2001).

^o Stellar temperature of CRL 2688 obtained from Zhang et al. (2013).

Table 2. Molecular transitions detected in CRL 2688 and IRC+10216 in the 20–25 GHz frequency range.

Frequency (MHz)	Species	Transition	CRL 2688			IRC+10216				
			rms (mK)	T_A^* (K)	$\int T_A^* dv^\dagger$ (K km/s)	Δv_{FWZI}^\dagger (km/s)	rms (mK)	T_A^* (K)	$\int T_A^* dv^\dagger$ (K km/s)	Δv_{FWZI}^\dagger (km/s)
21301.3	HC ₅ N	8 – 7	5	0.034	0.85±0.29	58.4	8	0.083	2.27±0.51	63.3
23963.9	HC ₅ N	9 – 8	6	0.033	0.88±0.22	36.5	8	0.119	3.23±0.55	68.8
20303.9	HC ₇ N	18 – 17	6	0.014	0.32:	50.5:	6	0.025	0.64±0.26	42.8
21431.0	HC ₇ N	19 – 18	5	0.013	0.36:	68.0:	8	0.028	0.58±0.32	40.6
22559.9	HC ₇ N	20 – 19	11	0.016	0.36:	48.8:	5	0.028	0.77±0.42	83.7
23687.9	HC ₇ N	21 – 20	6	0.018	0.38±0.26	43.0	8	0.038	1.03±0.48	59.5
24815.9	HC ₇ N	22 – 21	6	0.014	0.37:	53.2:	5	0.036	0.96±0.34	68.9
23694.5	NH ₃	1 (1) – 1 (1)	6	0.031	0.74±0.46	77.2	8	0.014	0.26:	55.7:
23722.6	NH ₃	2 (2) – 2 (2)	6	0.016	0.50:	55.6:	8
23870.1	NH ₃	3 (3) – 3 (3)	6	0.022	0.75±0.40	67.4	8
24139.4	NH ₃	4 (4) – 4 (4)	6	0.012	0.43:	78.9:	6

† Marginal detections are annotated with a colon (:).

Table 3. Hydrogen and helium recombination lines in NGC 7027.

Transition	Frequency (MHz)	rms (mK)	T_R (K)	$\int T_R dv^\dagger$ (km s ⁻¹ K)	$\Delta v_{\text{FWHM}}^\dagger$ (km s ⁻¹)
H 64 α	24509.9	18	0.17	6.02 \pm 1.72	33.9
H 65 α	23404.3	13	0.11	2.98 \pm 0.98	26.4
H 66 α	22364.2	15	0.11	5.21 \pm 1.67	39.8
H 67 α	21384.8	21	0.16	6.45 \pm 2.16	36.1
H 68 α	20461.8	20	0.15	5.17 \pm 1.86	35.7
H 81 β	23860.9	13	0.05	1.36 \pm 0.76	34.5
H 82 β	23008.6	13	0.05	1.18 \pm 1.03	52.1
H 95 γ	21964.3	13	0.03	0.60:	12.3:
He 64 α	24509.9	18	0.03	0.54:	43.0:
He 65 α	23413.8	13	< 0.02	< 0.80	...
He 66 α	22373.3	15	0.04	0.85:	28.4:
He 67 α	21393.6	21	0.04	1.02:	23.1:
He 68 α	20470.1	20	0.05	1.52:	77.2:

[†] Marginal detections are annotated with a colon (:).

Table 4. Excitation temperatures, column densities and fractional abundances with respect to molecular hydrogen of identified cyanopolyne molecules in CRL 2688 and IRC+10216.

Species	CRL 2688					
	T_{ex} (K)	δT_{ex} (\pm K)	N (10 ¹⁴ cm ⁻²)	δN (\pm 10 ¹⁴ cm ⁻²)	f_X ($\times 10^{-7}$)	δf_X ($\pm \times 10^{-7}$)
HC ₅ N ^a	24	1	2.6	0.4	0.6	0.1
HC ₇ N ^b	11	1	0.24	0.03	0.4	0.01
Species	IRC+10216					
	T_{ex} (K)	δT_{ex} (\pm K)	N (10 ¹⁴ cm ⁻²)	δN (\pm 10 ¹⁴ cm ⁻²)	f_X ($\times 10^{-7}$)	δf_X ($\pm \times 10^{-7}$)
HC ₅ N ^c	21	6	8	2	7	1
HC ₇ N	7	1

^aConcatenated with data from Zhang et al. (2013).

^bComputed with data points from the present survey alone.

^cConcatenated with data from Chau et al. (2012).

Table 5. Broad and narrow ammonia absorption features detected in the 20–25 GHz spectrum of CRL 618.

Transition	Frequency	Broad Absorption Features									
		T_A^* (mK)	δT_A^* (\pm mK)	V_{LSR} (km/s)	δV_{LSR} (\pm km/s)	Δ_{FWHM} (km/s)	$\delta \Delta_{\text{FWHM}}$ (\pm km/s)	Area (K km/s)	δ_{Area} (\pm K km/s)	$N_{J,K}$ (10^{12}cm^{-2})	$\delta_{N_{J,K}}$ ($\pm 10^{12} \text{cm}^{-2}$)
$J - K$											
1–1	23694.5	–32	7	–35	2	33	5	–0.9	0.1	49	3
2–2	23722.6	–26	7	–30	2	16	4	–0.48	0.09	19	1
3–3	23870.1	–30	7	–35	1	19	2	–0.66	0.08	23	1
4–4	24139.4	–12	7	–36	6	30	10	–0.4	0.2	14	2
5–5	24533.0
6–6	25056.0	–14	7	–30	10	80	30	–0.6	0.2	20	2
Transition	Frequency	Narrow Absorption Features [†]									
$J - K$											
1–1	23694.5
2–2	23722.6	–31	7	–6:	...	2:	...	–0.2:	...	6	...
3–3	23870.1	–45	7	–6.4	0.4	6.1	0.8	–0.37	0.04	13	1
4–4	24139.4	–41	7	–5	1	4	1	–0.23	0.06	7	1
5–5	24533.0	–44	7	–4.6	0.4	4.7	0.7	–0.27	0.04	8.4	0.5
6–6	25056.0	–43	7	–4.5	0.5	5	1	–0.25	0.04	8	1

[†] Marginal detections are annotated with a colon (:).

Table 6. Excitation temperature and column density of ammonia molecules detected in the 20–25 GHz NRO spectrum of CRL 618.

Component	T_{ex} (K)	δT_{ex} (\pm K)	N (10^{14} cm^{-2})	δ_N ($\pm 10^{14} \text{ cm}^{-2}$)
Broad absorption (low T_{ex} region)	28	10	3.6	0.5
Broad absorption (high T_{ex} region)	400	200	10	2
Narrow absorption	290	70	4.4	0.8

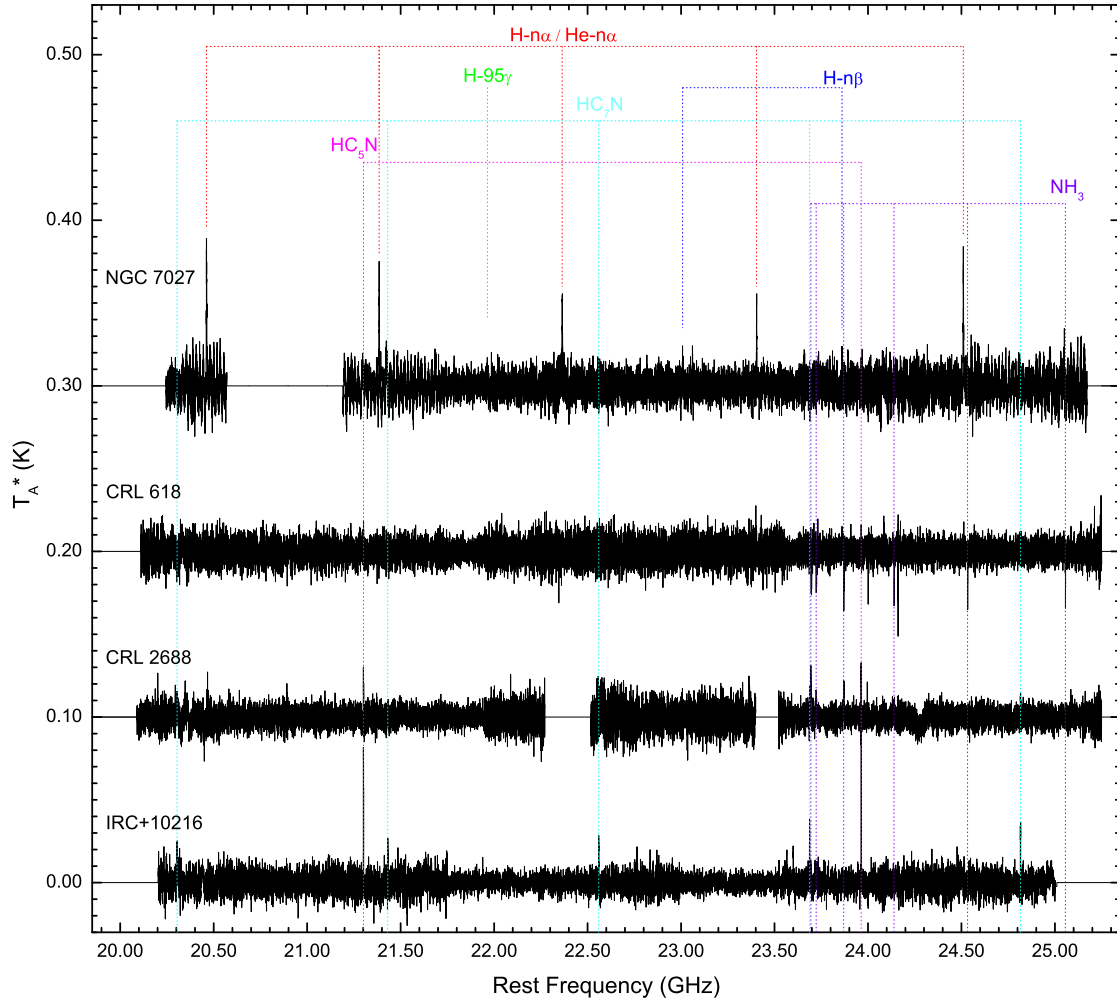


Fig. 1.— The 20–25 GHz spectra of IRC+10216, CRL 2688, CRL 618 and NGC 7027. Each subsequent spectra have been shifted upward by 0.1 K. Spectra of CRL 618 and NGC 7027 had been scaled by a factor of 0.8 and 0.5 respectively to match the rms of the other spectra. Identified spectral features are indicated accordingly. Note that the spectral regions with irregular baselines have been discarded.

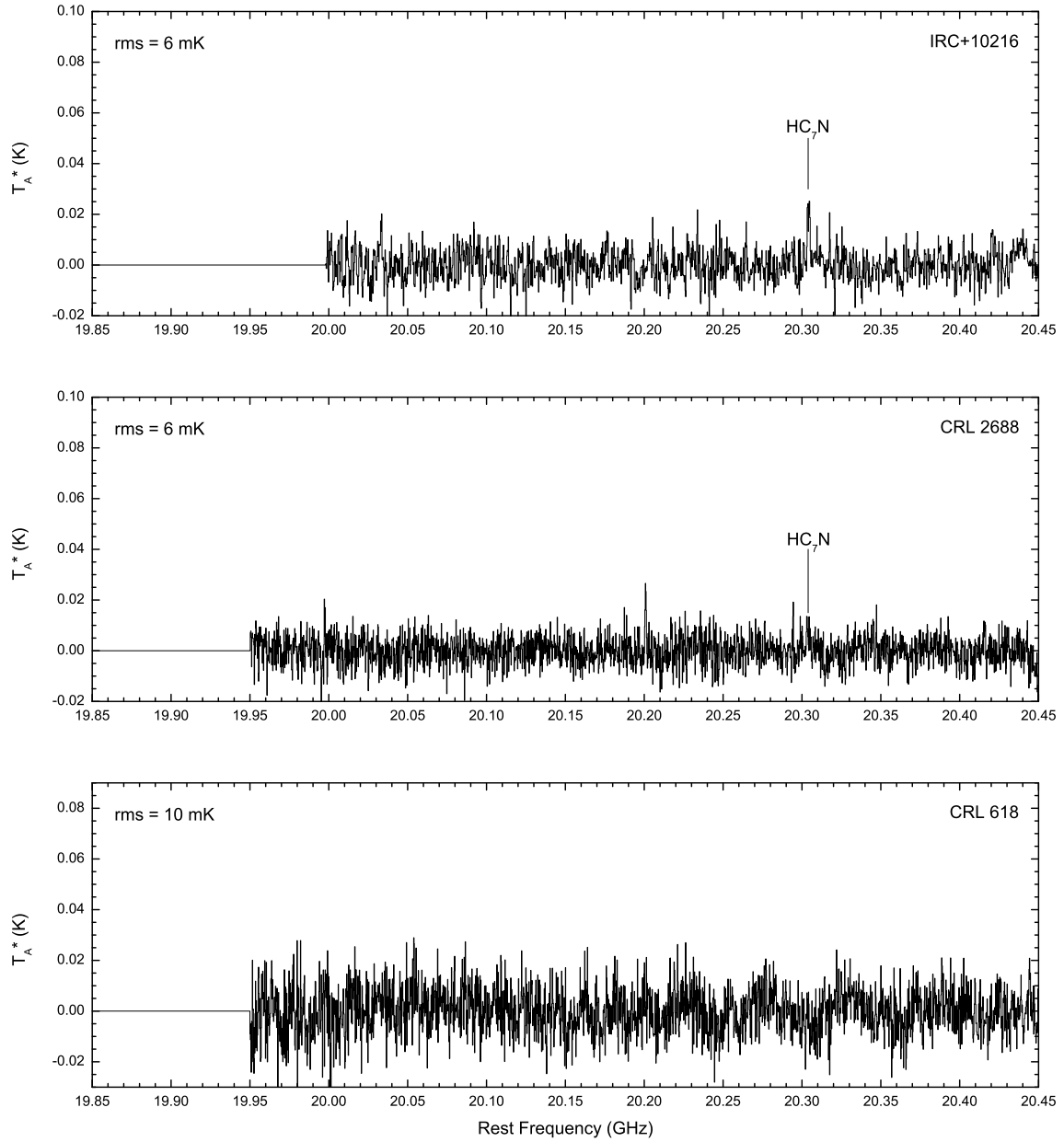


Fig. 2.— The reduced 20–25 GHz NRO spectra of IRC+10216, CRL 2688, CRL 618, and NGC 7027. The rms level of each region is shown. Positively identified features have also been labelled for ease of reference.

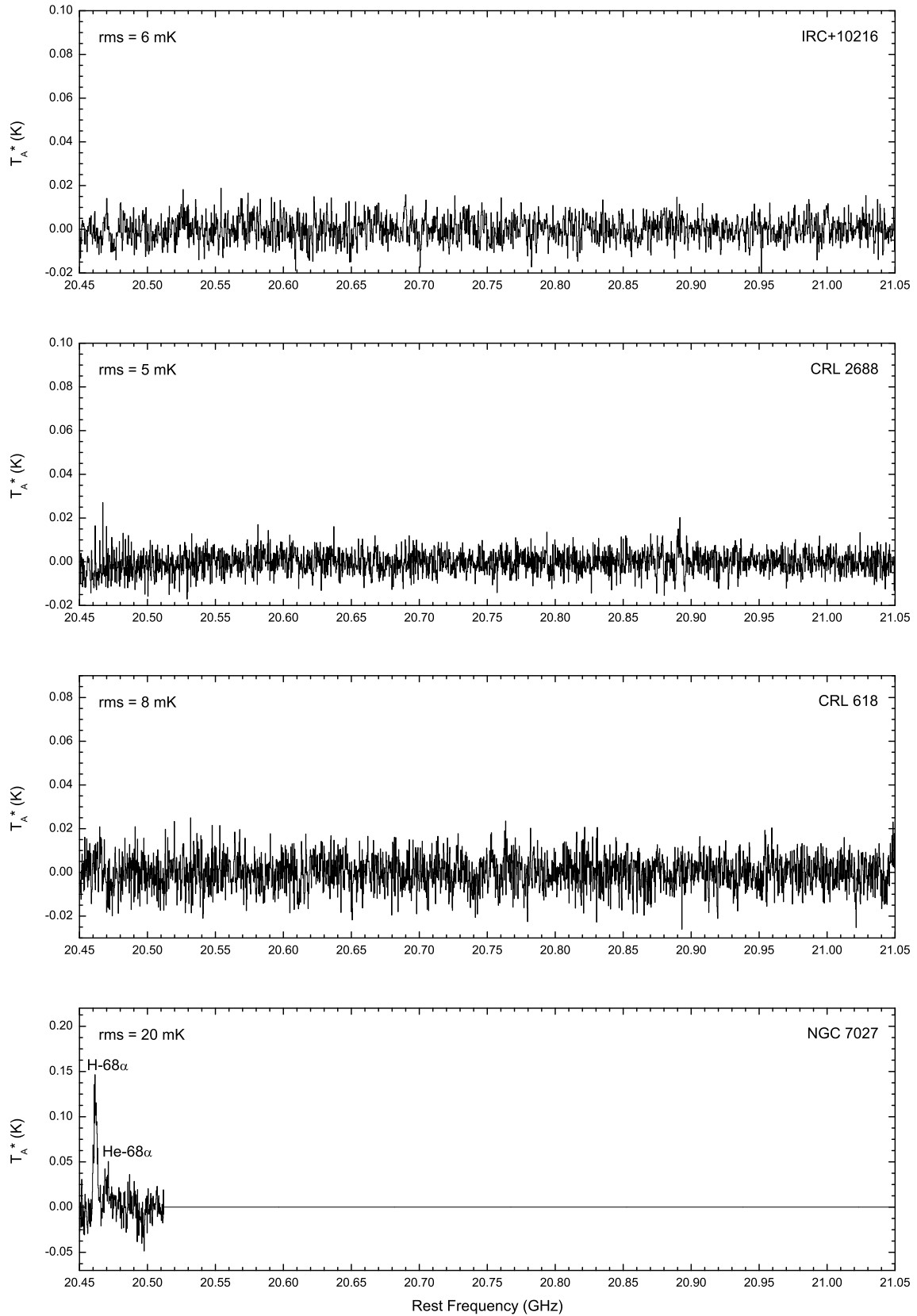


Fig. 2.— (continued)

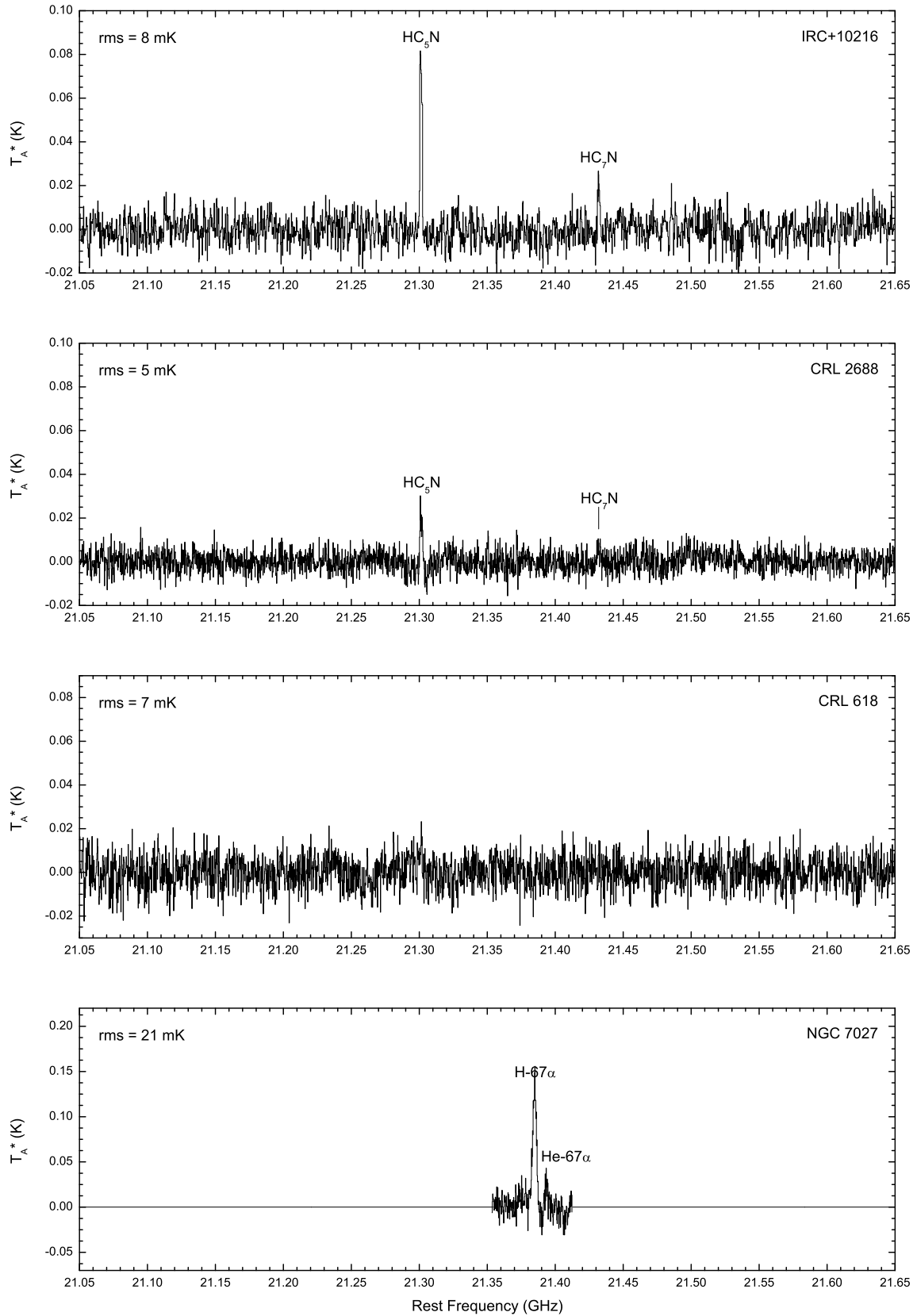


Fig. 2.— (continued)

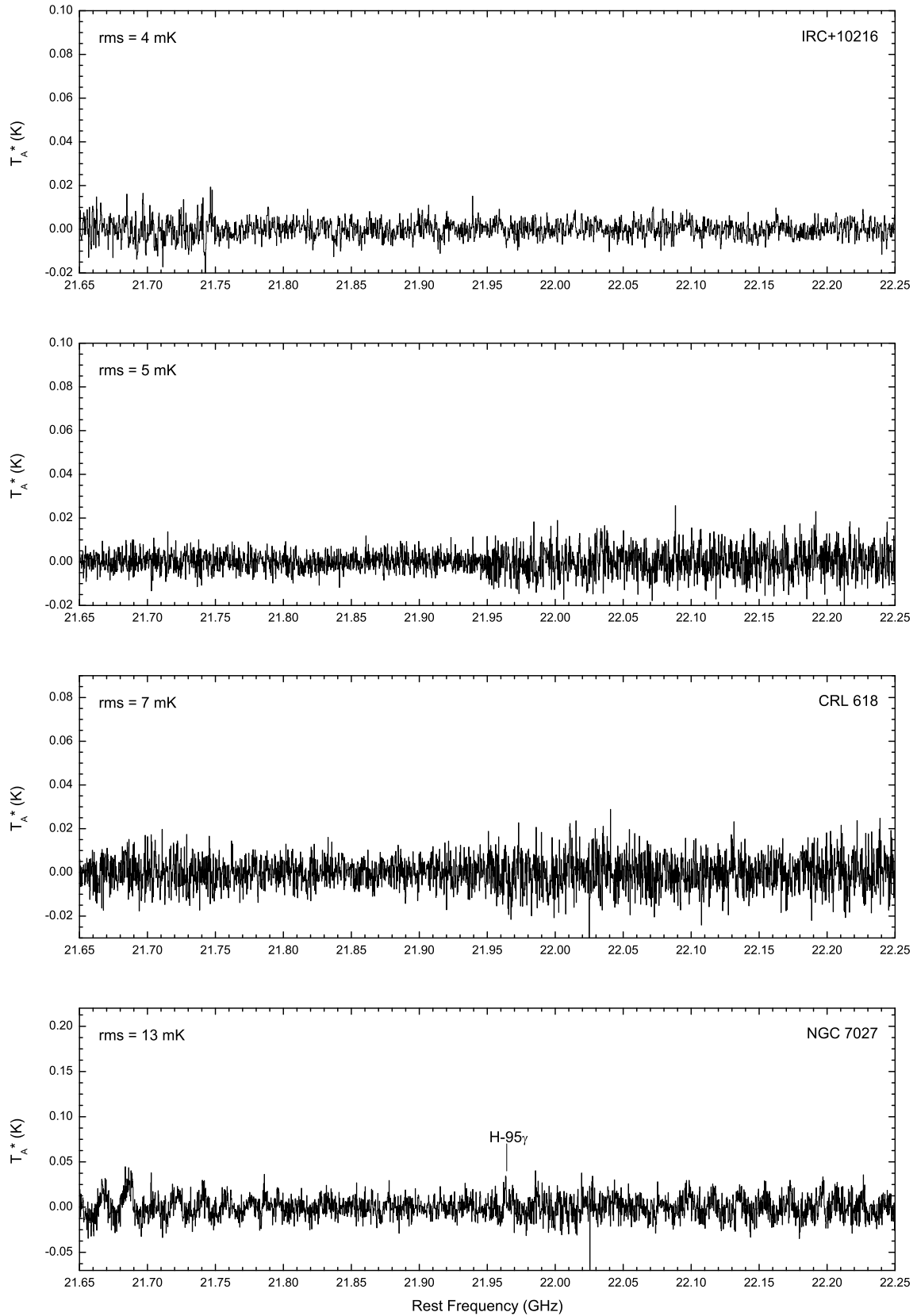


Fig. 2.— (continued)

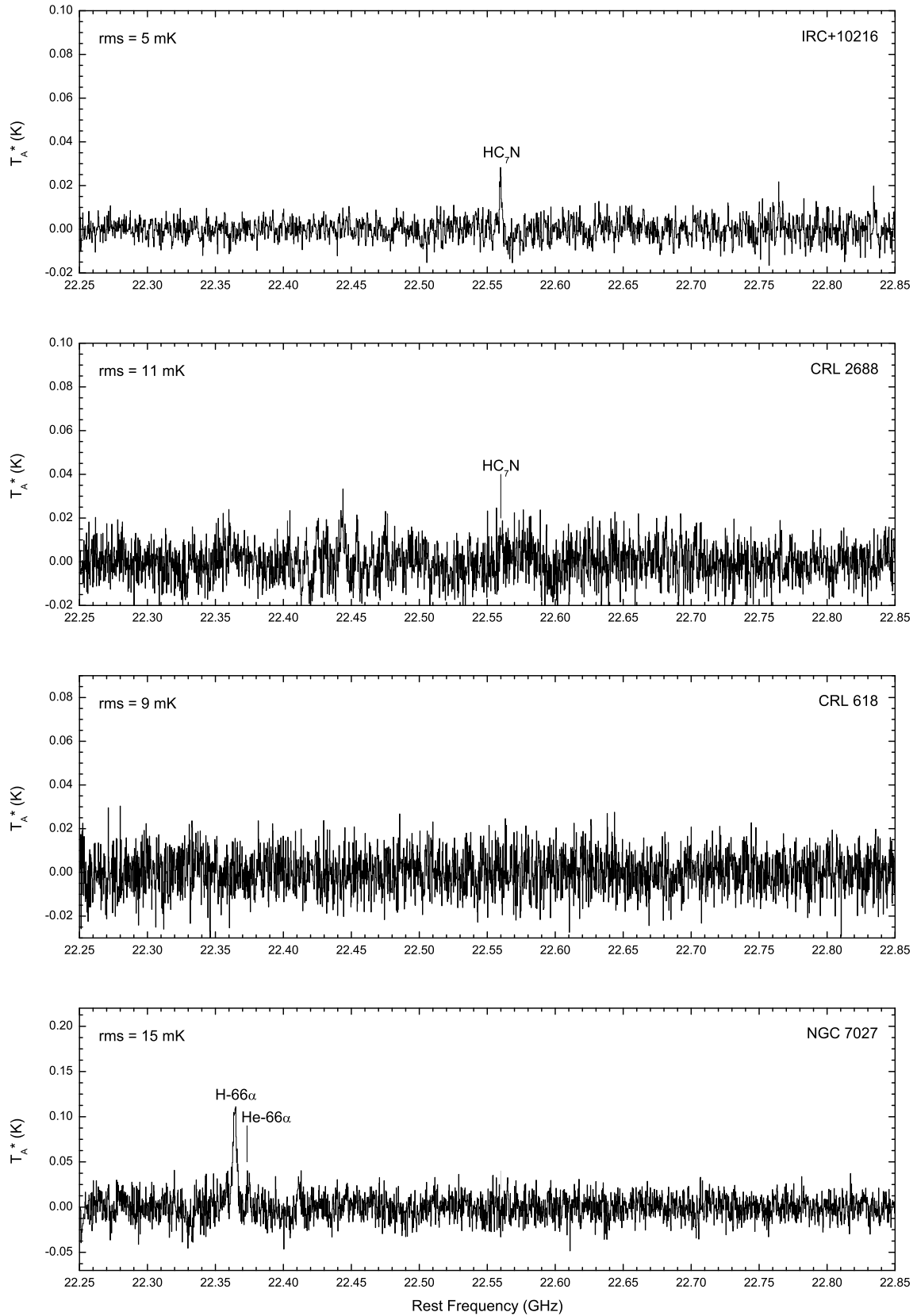


Fig. 2.— (continued)

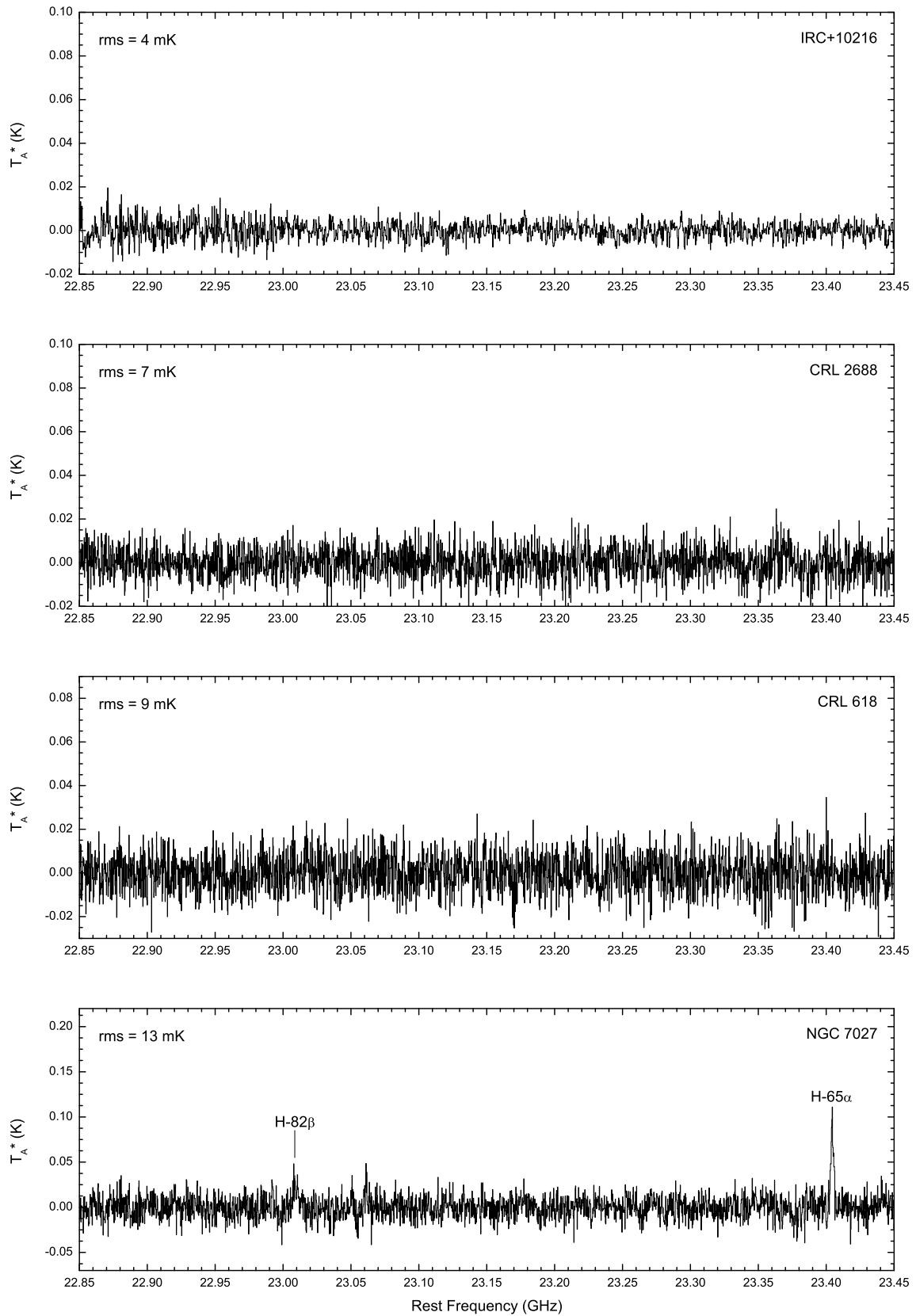


Fig. 2.— (continued)

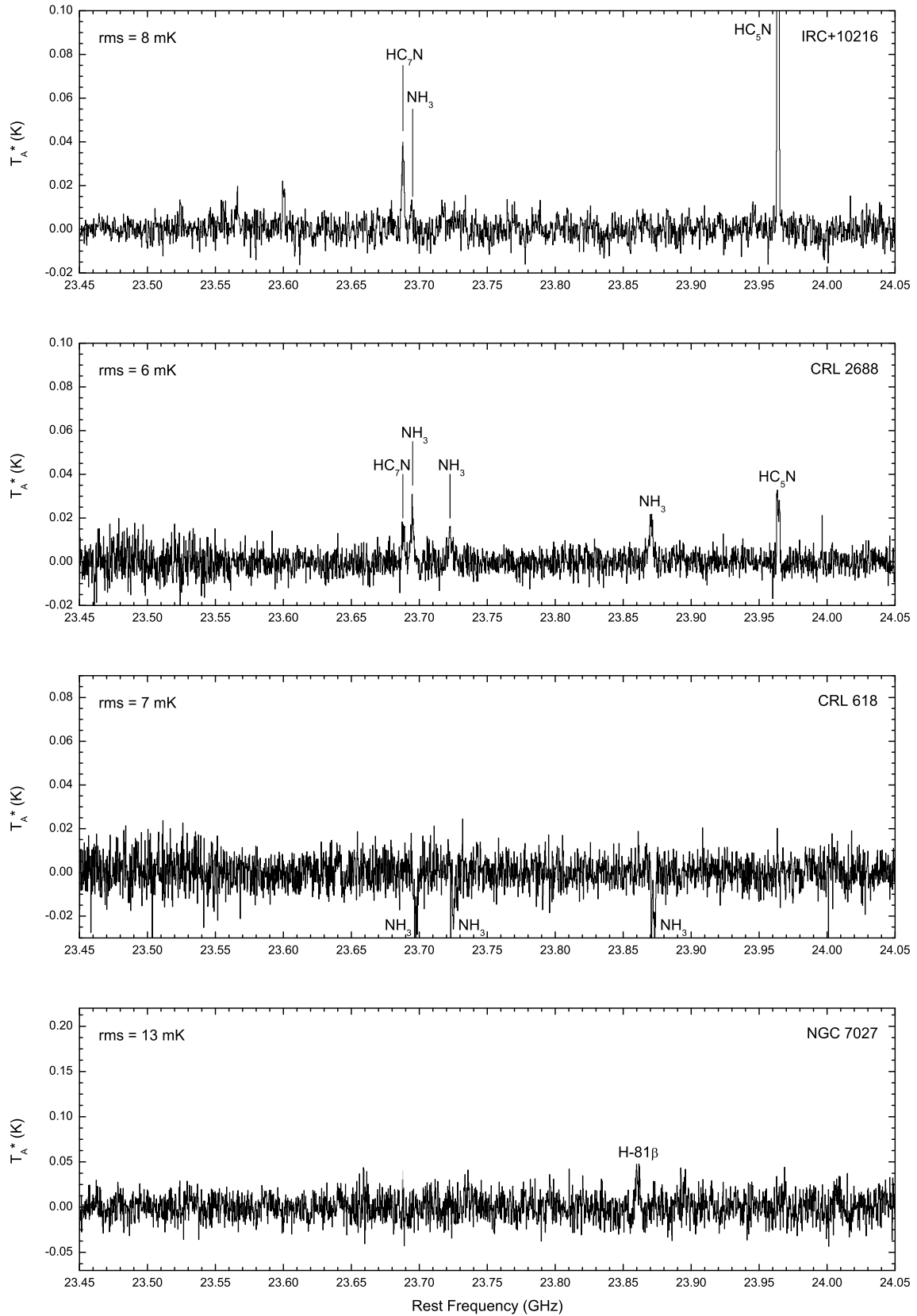


Fig. 2.— (continued)

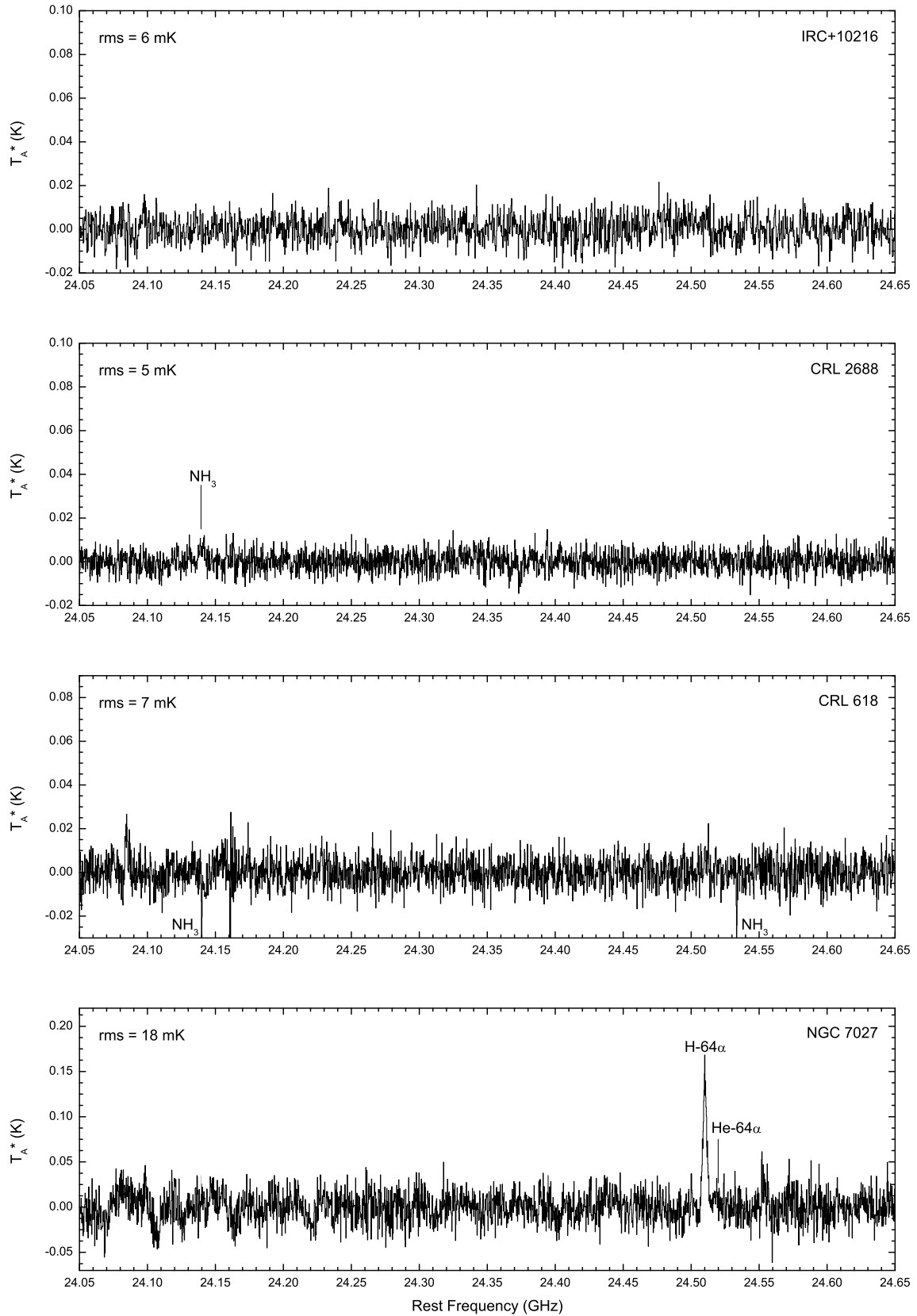


Fig. 2.— (continued)

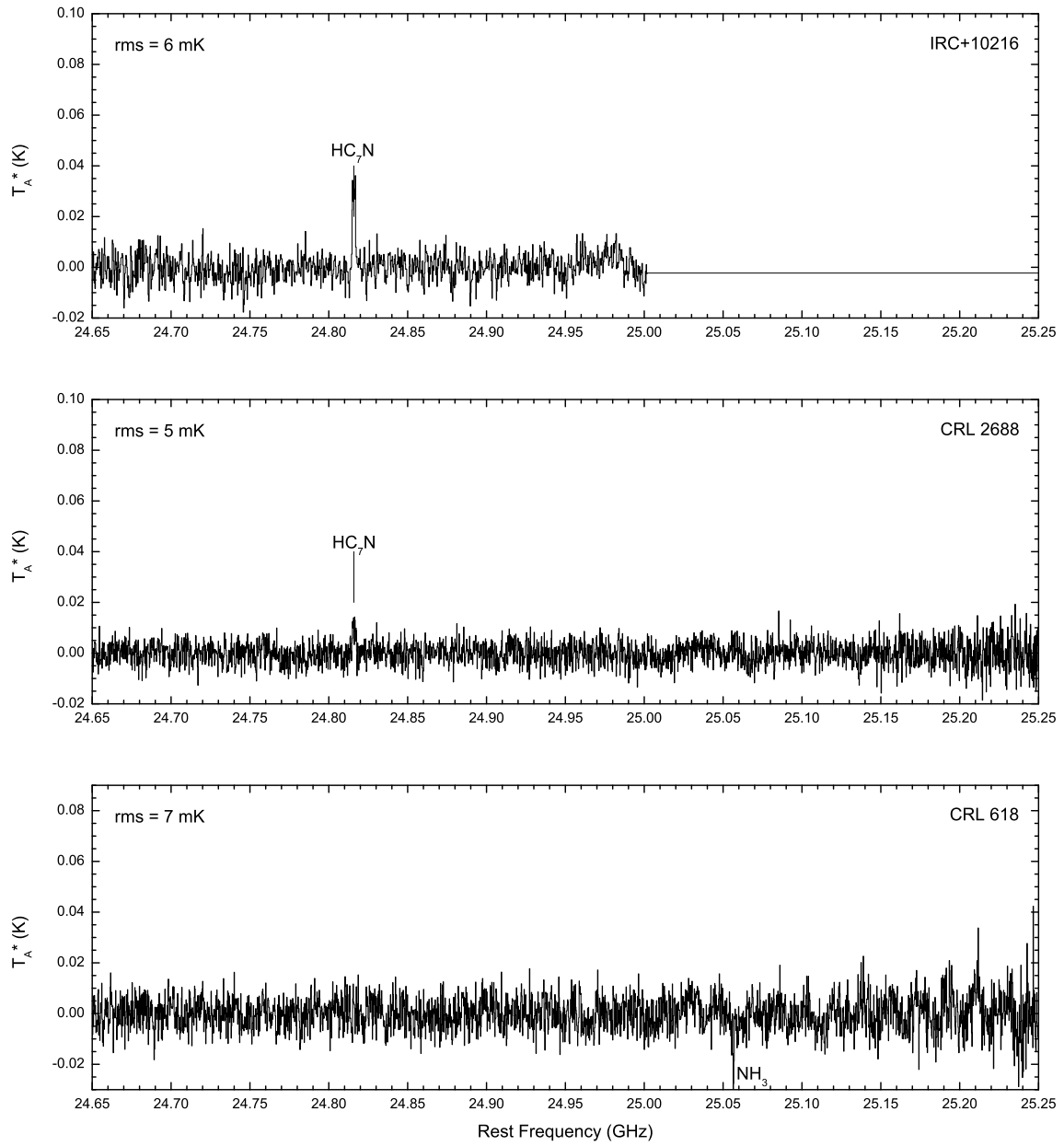


Fig. 2.— (continued)

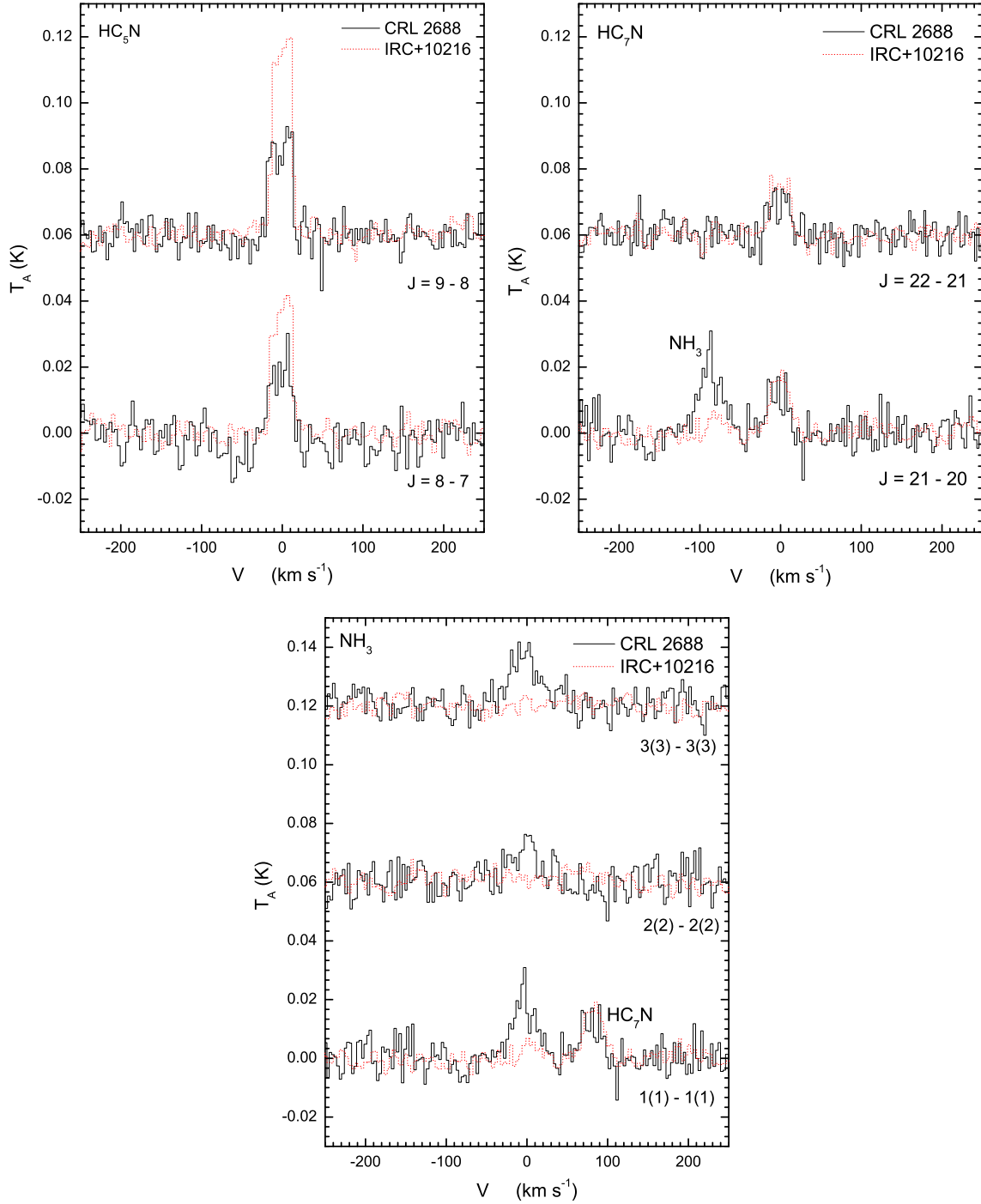


Fig. 3.— Line profiles of the prominent lines detected in the 20–25 GHz spectrum CRL 2688. The same lines identified in the spectrum of IRC+10216 have been scaled by 0.5 and superimposed on the CRL 2688 profiles. **The X-axis is given in $V_{\text{LSR}} - V_{\text{SYS}}$.**

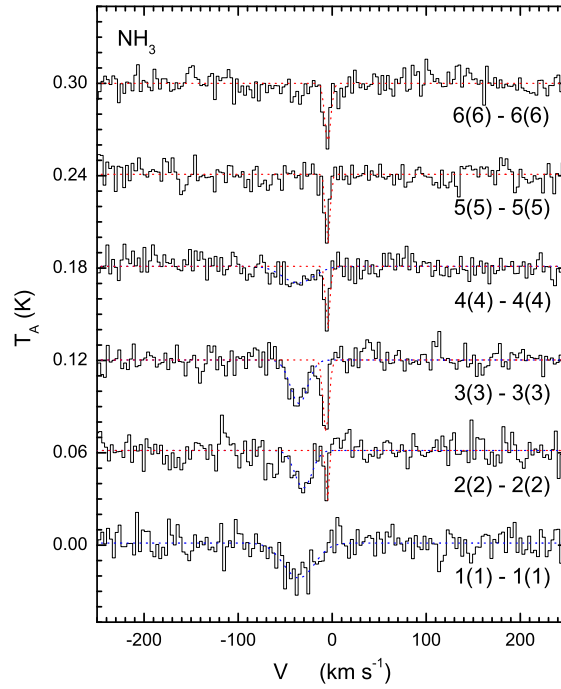


Fig. 4.— Profiles of NH_3 absorption features in the 20–25 GHz spectrum of CRL 618. Fittings of the broad (*blue*) and narrow (*red*) components are indicated by the dotted lines. **The X-axis is given in $V_{\text{LSR}} - V_{\text{SYS}}$.**

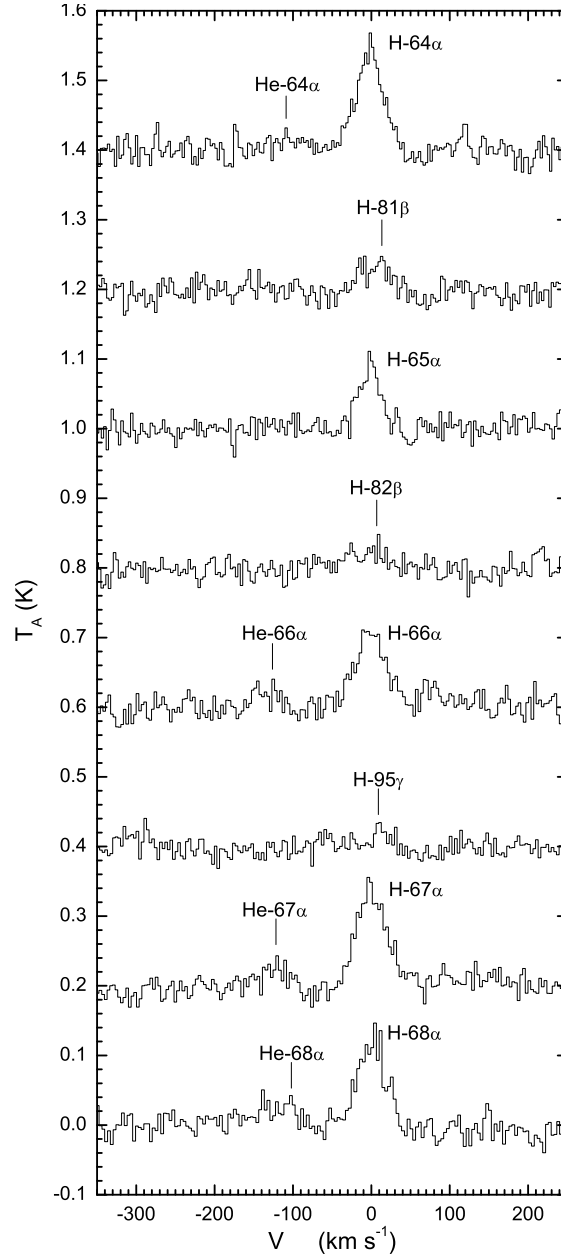


Fig. 5.— The profiles of hydrogen and helium recombination lines in the 20–25 GHz spectrum of NGC 7027. Profiles are arranged from top to bottom in terms of descending rest frequency. **The X-axis is given in $V_{\text{LSR}} - V_{\text{SYS}}$.**

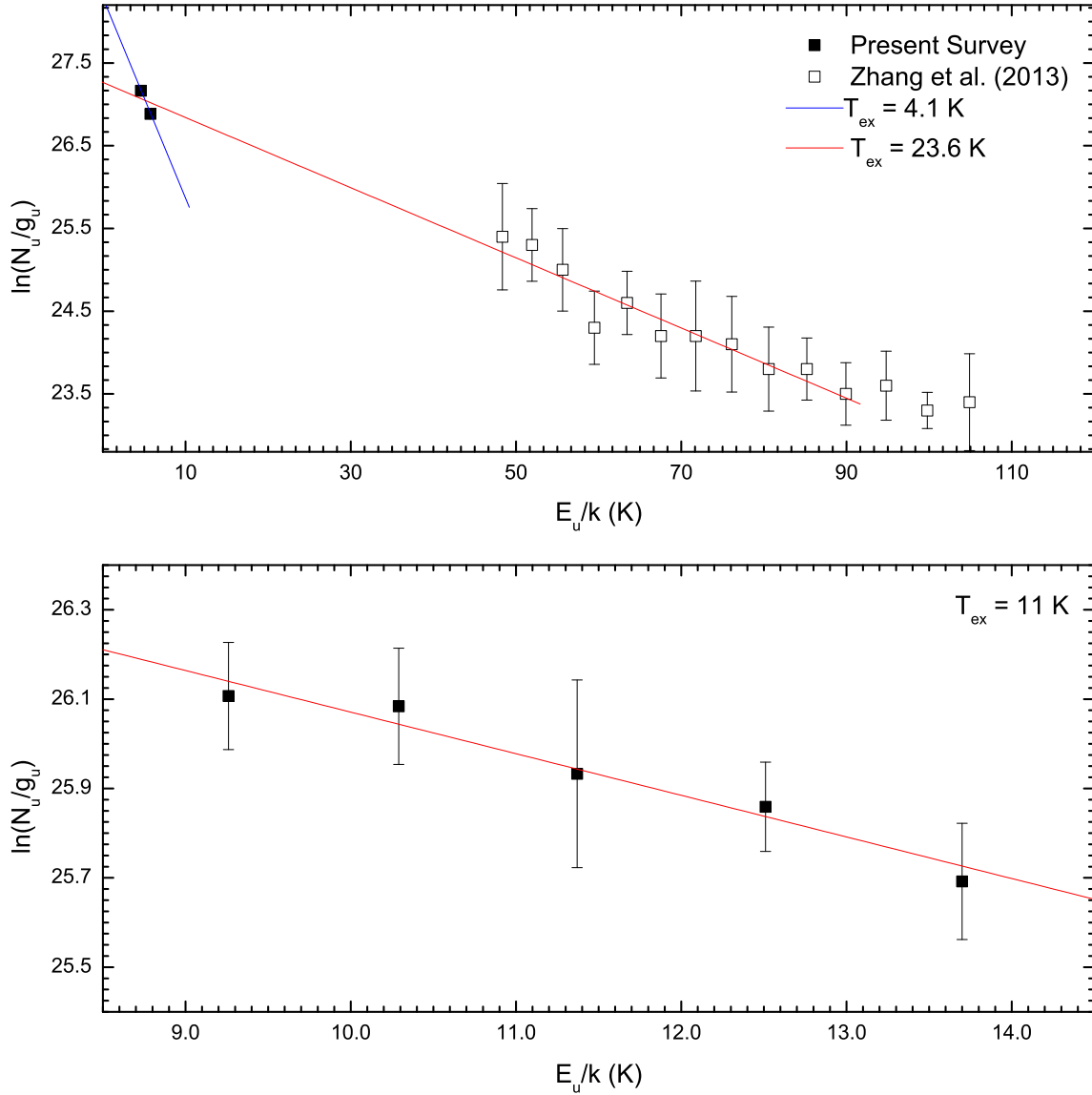


Fig. 6.— Rotational diagrams of cyanopolyynes molecules detected in the NRO spectrum of CRL 2688. *Upper panel:* Rotational diagram of HC₅N. Data points of HC₅N from Zhang et al. (2013) have been concatenated with data from the present study. *Lower panel:* Rotational diagram of HC₇N.

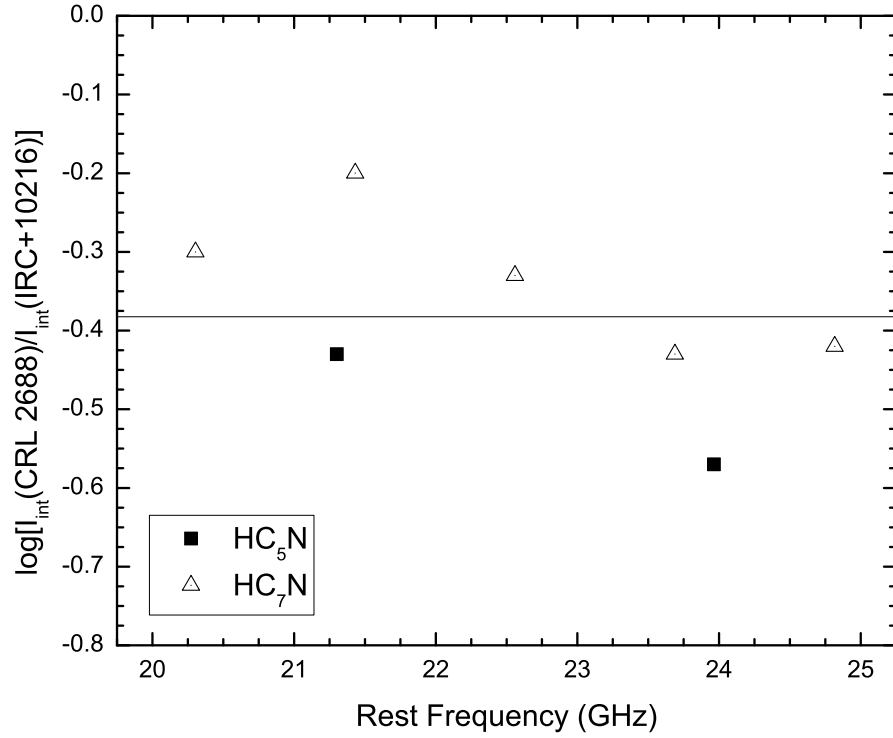


Fig. 7.— Integrated intensity ratios of detected cyanopolyynes between CRL 2688 and IRC+10216 after correcting for beam dilution. Ratios are presented on a logarithmic scale. The mean intensity ratio (0.41) is indicated by the solid line.

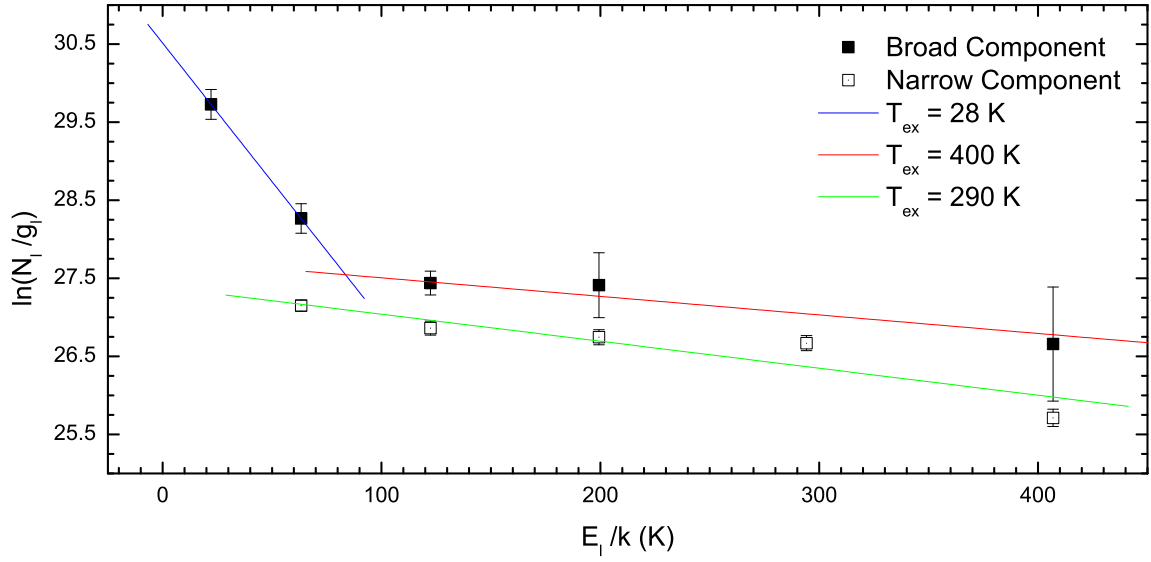


Fig. 8.— Rotational diagram for ammonia in CRL 618. The broad absorption and the hot clump regions are treated as separate components. The broad absorption component cannot be characterized by a single excitation temperature.